Eur. Phys. J. C 47, 395–411 (2006)
Digital Object Identifier (DOI) 10.1140/epjc/s2006-02574-x

THE EUROPEAN PHYSICAL JOURNAL C

Measuring the photon fragmentation function at HERA

A. Gehrmann-De Ridder[1,a], T. Gehrmann[2], E. Poulsen[2]

[1] Institute for Theoretical Physics, ETH, 8093 Zürich, Switzerland
[2] Institut für Theoretische Physik, Universität Zürich, Winterthurerstrasse 190, 8057 Zürich, Switzerland

Received: 5 April 2006 /
Published online: 16 June 2006 –

Abstract. The production of final state photons in deep inelastic scattering originates from photon radiation off leptons or quarks involved in the scattering process. Photon radiation off quarks involves a contribution from the quark-to-photon fragmentation function, corresponding to the non-perturbative transition of a hadronic jet into a single, highly energetic photon accompanied by some limited hadronic activity. Up to now, this fragmentation function was measured only in electron–positron annihilation at LEP. We demonstrate by a dedicated parton-level calculation that a competitive measurement of the quark-to-photon fragmentation function can be obtained in deep inelastic scattering at HERA. Such a measurement can be obtained by studying the photon energy spectra in $\gamma+(0+1)$-jet events, where γ denotes a hadronic jet containing a highly energetic photon (the photon jet). Isolated photons are then defined from the photon jet by imposing a minimal photon energy fraction. For this so-called democratic clustering approach, we study the cross sections for isolated $\gamma+(0+1)$-jet and $\gamma+(1+1)$-jet production as well as for the inclusive isolated photon production in deep inelastic scattering.

1 Introduction

The production of final state photons at large transverse momenta in high energy processes provides an important testing ground for QCD. A good understanding of the standard model predictions for photon production is essential for new physics searches at future colliders. In high energy collisions, the produced primary partons, quarks or gluons, subsequently fragment into clusters of comoving hadrons, the hadronic jets. In events where a photon is produced in addition to the jets, this photon can have two possible origins: the direct radiation of a photon off a primary quark or antiquark (or, if leptons are also involved in the process, off a charged lepton) and the fragmentation of a hadronic jet into a photon carrying a large fraction of the jet energy. While the former direct process takes place at an early stage in the process of hadronisation and can be calculated in perturbative QCD, the fragmentation contribution is primarily due to a long-distance process which cannot be calculated within perturbative method. The latter is described by the process-independent quark-, antiquark- or gluon-to-photon fragmentation functions [1] which must be determined by experimental data. Their evolution with the factorisation scale $\mu_{\mathrm{F},\gamma}$ can however be calculated perturbatively. Furthermore, when the photon is radiated somewhat later during the hadronisation process, in addition to this genuinely non-perturbative fragmentation process, the emission of a photon collinear to the primary quarks can also take place and has to be taken into account. As physical cross sections are necessarily finite these collinear divergences will get factorised into the fragmentation functions. The factorisation procedure of these final state collinear singularities in fragmentation functions used here is of the same type as the procedure used to absorb initial state collinear singularities [2] into the parton distribution functions.

Directly produced photons are usually well separated from the hadronic jets produced in the event, while photons originating from the fragmentation process and collinear quark–photon emission are primarily found inside hadronic jets. Consequently, it was thought that by imposing some isolation criterion one could eliminate the fragmentation process and define isolated photon events in this way. However this is not the case: one can at most suppress the fragmentation and collinear contributions. In most theoretical observables involving final state photons, those contributions are indeed present.

So far, only a limited number of measurements of single photon production exists through which direct information on the quark-to-photon fragmentation function (denoted by FF) can be obtained. A possible way is the measurement of inclusive photon cross sections in different experimental environments. The OPAL Collaboration measured the inclusive photon rate [3] in e^+e^- annihilation for $0.2 < x_\gamma < 1.0$ where in terms of the beam energy $x_\gamma = 2E_\gamma/M_Z$ is the photon energy fraction. The results were in reasonable agreement with predictions obtained using various model estimates of photon fragmentation functions for which the factorisation scale $\mu_{\mathrm{F},\gamma}$ was chosen to be equal to M_Z [4–6]. The experimental precision was however not suf-

[a] e-mail: gehra@itp.phys.ethz.ch

ficiently high to discriminate between different theoretical predictions.

An alternative way to determine the process-independent photon fragmentation function is to measure the production of photons accompanied by a definite number of hadronic jets. It should be noted that the quark-to-photon fragmentation function determined via the measurement of inclusive or jet-like observables is the same in both cases as it is process-independent. Indeed the fragmentation process and the collinear quark–photon emission are found inside the hadron jets and those contributions are the same whether one analyses inclusive or jet-like observables.

In processes involving hadronic jets and a photon in the final state, the outgoing photon is treated like any other hadron by the jet algorithm. It is clustered simultaneously with the other hadrons into jets, within the so-called democratic procedure [7, 8]. One of the jets will contain a photon and will be called photon-jet if the fraction of energy carried by the photon z inside the jet is sufficiently large, i.e.

$$z = \frac{E_\gamma}{E_\gamma + E_{\rm had}} > z_{\rm cut} \,, \tag{1}$$

with $z_{\rm cut}$ fixed experimentally. z can also be defined with respect to the transverse energies instead of the energies.

Following this line, the ALEPH Collaboration [8] has analysed events produced on the Z-resonance in e^+e^- collisions which contained one hadron jet and one photon jet, where the photon carried at least 70% of the jet energy. A comparison between the measured rate and a leading order (LO), $\mathcal{O}(\alpha)$, calculation [7] yielded a first determination of the quark-to-photon fragmentation function in observables related to jets. It is worth noting that in this observable, called the $\gamma+1$-jet rate, the quark-to-photon fragmentation function appears already at the lowest order. This observable is therefore highly sensitive on the quark-to-photon fragmentation function and particularly suited to determine it. The calculation of the $\gamma+1$-jet rate was furthermore extended to next-to-leading order (NLO), i.e. up to $(\mathcal{O}(\alpha\alpha_{\rm s}))$ in [9] and a NLO fragmentation function was obtained [10] by comparison with the ALEPH data. Computing the inclusive photon rate in the same fixed-order framework with the LO and NLO fragmentation functions obtained from the ALEPH data, one finds [11] that the results are in good agreement with the OPAL measurement [3].

To define isolated photons produced in a hadronic environment, a minimal amount of hadronic activity close to the photon must be admitted to ensure the infrared finiteness of the observable. In the approach followed by ALEPH, the isolated photon rate is defined as the $\gamma+1$-jet rate where the photon carries 95% of the photon-jet energy. The amount of energy required for a photon inside the photon-jet to be called "isolated" was fixed by analysing the data on the $\gamma+1$-jet rate for $0.7 < z < 1$. The amount fixed depends on the experimental context. In [8], the calculated and measured isolated rates were compared while varying the jet clustering parameter $y_{\rm cut}$. The theoretical prediction for the isolated rate defined as the $\gamma+$ 1-jet rate for $z > 0.95$ using the measured photon fragmentation function at a given value of $y_{\rm cut}$ were found in agreement with the measured isolated rate over the whole range of $y_{\rm cut}$. The inclusion of the NLO corrections in the theoretical prediction improved the agreement.

Photon isolation from hadrons has been discussed intensively in the literature [12], and up to now the most common procedure uses a cone-based isolation criterion following the Snowmass convention [13]. Recently, the ZEUS Collaboration [14] performed a measurement of the inclusive isolated photon production cross section in electron–proton deep inelastic scattering (DIS) at HERA using a cone-based isolation procedure. In this cross section, the photon carried 90% of the energy inside a cone defined in rapidity and azimuthal angle around the photon. In [14], this measurement was compared to predictions obtained with the Monte Carlo parton shower event generator programs PYTHIA [15] and HERWIG [16], which do not include photon fragmentation. ZEUS observed a noticeable excess of the measurement compared to the predictions. Moreover, even after rescaling the normalisation of the cross section, none of the programs was able to describe all kinematical distributions of the experimental data in a satisfactory manner.

It was suggested in [17] that the isolated photon production cross section in DIS could be used to determine the photon distribution in the proton, assuming that all observed isolated photons are radiated from the lepton only. This photon distribution inside the proton is an important ingredient to electroweak corrections to cross sections at hadron colliders [18]. Although the observed total cross section seemed to be in agreement with model estimates based on QED-generated photon distributions in the proton [19], it was recently demonstrated [20] that the kinematical distribution of photons inside the proton cannot be described in this approach.

In [21], we performed a dedicated parton-level calculation of the observable measured by ZEUS, using the same cone-based isolation criterion as the ZEUS Collaboration to define the isolated photon cross section. This parton-level calculation naturally includes two aspects which are neglected in the event generators: quark-to-photon fragmentation and large angle radiation of the photon from the lepton or from the quark. Our results were found in good agreement with all aspects of the experimental measurement.

In addition to measuring the inclusive isolated photon cross section, the ZEUS Collaboration also analysed [14] the production of prompt photons in association with hadronic jets. This measured cross section was then compared with the NLO calculation [22] of the $\gamma+(1+1)$-jet cross section: the cross section for the production of a photon-jet and one additional hadron-jet in the final state (n-jet observables in DIS are usually denoted by $(n+$ 1)-jet observables where the +1 stands for the unobserved jet coming from the proton remnant). Data and theory were found to be in good agreement.

For this observable however, the quark-to-photon fragmentation function enters only at the next-to-leading order. Indeed, the ZEUS Collaboration did not analyse their data in view of a determination of the quark-to-

photon fragmentation function but just compared data and theory for the $\gamma+(1+1)$-jet cross section.

To measure the quark-to-photon fragmentation function at HERA in DIS, it seems best to consider the analogue to the $\gamma+1$-jet rate at LEP, thus the $\gamma+(0+1)$-jet cross section. For this observable, besides the photon jet, no further hadronic jet activity is present in the final state except the proton remnant jet, of course. Moreover, the quark-to-photon fragmentation function enters at the lowest order. It is the principal goal of this paper to advocate a measurement of the quark-to-photon fragmentation function utilising HERA data on $\gamma+(0+1)$-jet events in DIS.

More precisely, the plan of the paper is as follows. In Sect. 2, we present the calculation of the $\gamma+(0+1)$-jet cross section which consists of the hard photon emission and the fragmentation process and we discuss how these two contributions are combined and implemented into a parton-level Monte Carlo program. Section 3 contains our predictions for the $\gamma+(0+1)$-jet cross section differential in z ($0.7<z<1$) using a given jet algorithm to build $\gamma+(0+1)$-jet final states, evaluated for different quark-to-photon fragmentation functions. We illustrate how a measurement of this differential cross section can be used to extract the quark-to-photon fragmentation function. Defining isolated photons in deep inelastic scattering by considering photon jets with $z>0.9$, in Sect. 4, we present our results for the isolated $\gamma+(0+1)$-jet cross section and the isolated inclusive photon cross section, differential in rapidity (η_γ) and transverse energy ($E_{\mathrm{T},\gamma}$). These are studied for different jet algorithms. Finally, Sect. 5 contains the conclusions and an outlook.

2 Parton-level calculation

We consider the production of $\gamma+(0+1)$ jets in DIS. $\gamma+(0+1)$ jets are understood as a final state containing a highly energetic photon, which can be part of a hadronic jet (called the photon-jet and abbreviated by "γ"), no further jet ("+0") except the remnant jet ("+1"). At leading order, the photon production process in DIS is $\mathcal{O}(\alpha^3)$ which is to be compared with $\mathcal{O}(\alpha^2)$ for the inclusive deep-inelastic process. At this order, two different partonic processes yield $\gamma+(0+1)$-jet final states. (a) $lq\to lq\gamma$, where the photon and the quark are either clustered together into a single jet ($z<1$) or the quark is well separated from the photon, but is at too low transverse momentum or at too large rapidity to be identified as a jet ($z=1$). (b) $lq\to lq$, where the quark jet fragments into a highly energetic photon carrying a large fraction z of the jet energy.

Both processes will be discussed in detail in the following subsections. Following those, we will describe how the two contributions are combined and implemented in a numerical parton-level Monte Carlo program.

2.1 Kinematical definition of the observable

To select $\gamma+(0+1)$ jets in DIS, several criteria must be fulfilled by the final state particles: deep inelastic scattering events (as opposed to photoproduction, [23, 24]) are selected by requiring the final state electron to be observed in the detector. The final state electron carries an energy E_e and is observed at a scattering angle Θ_e (measured with respect to the incoming proton direction). These variables determine the common DIS variables y and Q^2. The kinematics of the final state photon are characterised by its transverse energy $E_{\mathrm{T},\gamma}$ and its rapidity η_γ (which may be inferred respectively from the transverse energy and the rapidity of the photon jet, defined by a jet algorithm). Finally, to avoid contributions from elastic Compton scattering $ep\to ep\gamma$, several hadronic tracks are required in the detector.

To define the $\gamma+(0+1)$ jet cross section in DIS, numerous cuts on the kinematical variables for the final state electron and photon momenta are applied to preselect candidate events. In the following, we denote these cuts collectively by $\Theta(p_e,p_\gamma)$. The selected events are then subjected to a jet algorithm, which combines $n-1$ observed particle momenta, including the photon, and the proton remnant, (whose momentum p_n is inferred from momentum conservation), into a $\gamma+(0+1)$-jet final state. We denote the action of this jet algorithm onto the n final state momenta symbolically by a jet function $J^{(n)}_{\gamma+(0+1)}(p_1,\dots,p_n)$.

2.2 Hard photon emission processes

At leading order, $\mathcal{O}(\alpha^3)$, the cross section for the production of hard photons in DIS is described by the quark (antiquark) process

$$l(p_1)+q(p_2)\to\gamma(p_3)+l(p_4)+q(p_5)$$

with the particle momenta given in parentheses. l denotes a lepton or antilepton, and q a quark or an antiquark. The momentum of the incoming quark is a fraction ξ of the proton momentum P, $p_2=\xi P$ and the proton remnant r carries the momentum $p_r=(1-\xi)P$. The latter hadronises into the remnant jet independently of the other final state particles. The contribution of this process to the $\gamma+(0+1)$-jet cross section is given by the integral over the three-parton final state phase space, weighted by the jet definition and the cuts:

$$\int \mathrm{d}PS_3\,|M|^2_{lq\to\gamma lq}\,J^{(3)}_{\gamma+(0+1)}(p_3,p_5,p_r)\,\Theta(p_3,p_4)\,. \qquad (2)$$

Both leptons and quarks emit photons. In the scattering amplitudes for this hard photon production process, depicted in Fig. 1, the lepton–quark interaction is mediated by the exchange of a virtual photon. The final state photon can be emitted off the lepton or off the quark. Consequently, one finds three contributions to the cross section, coming from the squared amplitudes for radiation off the quark (QQ) or the lepton (LL), as well as the interference of these amplitudes (QL). These contributions were computed originally as part of the QED radiative corrections to DIS [25], where the final state photon remains unobserved. The QL contribution is odd under charge exchange, such that it contributes with opposite sign to the cross sections with $l=e^-$ and $l=e^+$.

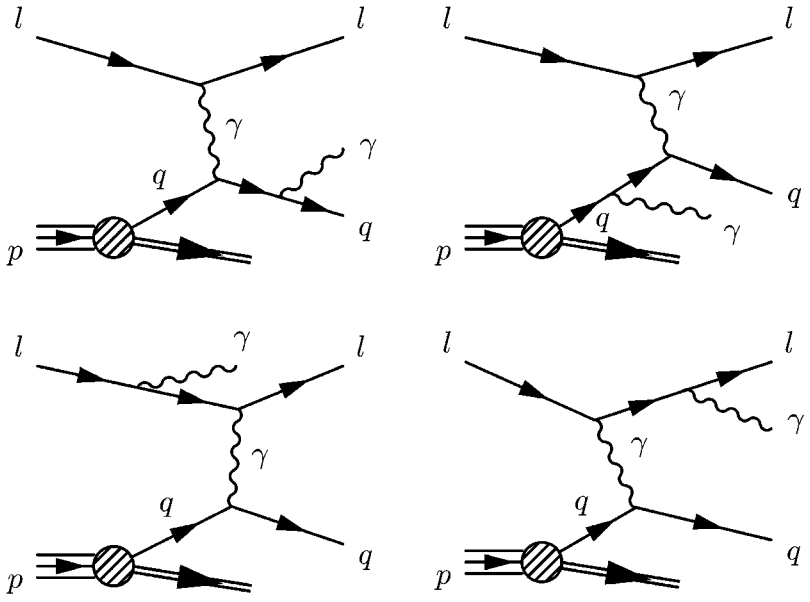

Fig. 1. Leading order Feynman amplitudes for hard photon production in DIS. The QQ-contribution is obtained by squaring the sum of the upper two amplitudes, the LL-contribution from the square of the lower two amplitudes, and QL-contribution from their interference

In the LL subprocess the final state photon is radiated off the lepton. Since the cuts ensure that photon and electron are experimentally separated, this subprocess is free of a collinear electron–photon singularity. As the photon is radiated off the lepton, the momentum of the final state lepton cannot be used to determine the invariant four-momentum transfer between the lepton and the quark, which is in this subprocess given by $Q^2_{LL} = -(p_5 - p_1)^2$, with $Q^2_{LL} < Q^2 = Q^2_{QQ} = -(p_4 - p_2)^2$. In principle, Q^2_{LL} is unconstrained by the kinematical cuts, and the squared matrix element for the LL subprocess contains an explicit $1/Q^2_{LL}$.

In this process, the requirement of observing hadronic tracks comes into play, since the limit $Q^2_{LL} \to 0$ corresponds to photon radiation in elastic electron–proton scattering (also called Compton scattering), $ep \to ep\gamma$. To translate the track requirement into parton-level variables, we proceed as discussed in [21]. The central tracking detectors of the HERA experiments cover in the forward region rapidities of $\eta < 2$. Requiring tracks in this region amounts to the current jet being at least partially contained in it. Assuming a current jet radius of one unit in rapidity, this amounts to a cut on the outgoing quark rapidity $\eta_q < 3$, which we apply here. Varying this cut results only in small variations of the resulting cross sections. The cut on the outgoing quark rapidity enforces a minimum for Q^2_{LL}, thus it avoids a singularity in this subprocess cross section $\hat{\sigma}_{LL}$.

Some care has to be taken in the choice of the factorisation scale for the quark distribution function inside the proton, μ^2_{F}, in the LL subprocess. In a leading order parton model calculation, μ^2_{F} should ideally be taken to be the invariant four-momentum transfer to the quark, i.e. Q^2_{LL} for the LL subprocess. Even applying the quark rapidity cut, Q^2_{LL} can assume low values, $Q^2_{LL} \sim \Lambda^2_{\mathrm{QCD}}$, where the parton model description loses its meaning. Because of the cuts, this kinematical region yields however only a small contribution to the cross section. To account for it in the parton model framework, we introduce a minimal factorisation scale $\mu_{\mathrm{F,min}} = 1\,\mathrm{GeV}$, and choose for the LL subprocess $\mu_{\mathrm{F}} = \max(\mu_{\mathrm{F,min}}, Q_{LL})$, and for the QL interference contribution $\mu_{\mathrm{F}} = \max(\mu_{\mathrm{F,min}}, (Q_{LL} + Q_{QQ})/2)$. This fixed factorisation scale is an approximation to more elaborate procedures to extend the parton model to low virtualities [27], but sufficient in the present context.

This procedure for the scale setting in the LL and QL subprocesses is similar to what is done in the related process of electroweak gauge boson production in electron–proton collisions [28]. The major difference to [28] is that the cross section for isolated photon production in DIS vanishes for $Q^2_{QQ,LL} \to 0$, while being non-vanishing for vector boson production. Consequently, in [28] the calculation of deep inelastic gauge boson production had to be supplemented by photoproduction of gauge bosons at $Q^2 = 0$, with a proper matching of both contributions at a low scale. This is not necessary in our case.

In the QQ contribution, the photon radiated from the quark can have been radiated at two different stages of the hadronisation process. The quark and the photon are usually well separated from each other if the radiation took place at an early stage, a process we shall name real hard emission. When the photon is radiated somewhat later during the hadronisation process, the emission of a photon collinear to the primary quarks can take place which gives rise to a collinear singularity in the calculation. Both contributions, hard and collinear emission processes, can be calculated within perturbative QCD as will be described below.

As physical cross sections are necessarily finite, the collinear singularity appearing in the collinear emission process gets factorised into the fragmentation function defined at some factorisation scale $\mu_{\mathrm{F},\gamma}$. The fragmentation process will be discussed in the next subsection.

In the real emission processes, the final state partons are experimentally unresolved, as quark and photon get clustered in one jet. Those partons can be theoretically

resolved, well separated from each other (real hard radiation) or they can be theoretically unresolved. In the latter case the quark and the photon are collinear (real collinear radiation). The calculation of these two contributions is performed using the phase space slicing method [26]. By introducing a parameter $y_{\min}$, one is able to separate the divergent, quark–photon collinear contribution from the finite contribution where the quark and the photon are theoretically separated.

The collinear contribution corresponds to the collinear limit of the matrix element integrated over the phase space region relevant to the collinear limit. This phase space region is defined by $y_{q\gamma} < y_{\min}$, where $y_{q\gamma} = s_{35}/s_{12}$ is the dimensionless invariant mass of the quark–photon system. Due to collinear factorisation of the phase space and the matrix element, the collinear contribution yields a universal collinear factor multiplied by the hard $2 \to 2$ cross section ($\hat{\sigma}_{eq\to eq}$). This divergent collinear factor is calculated analytically and absorbed into the quark-to-photon fragmentation function as we will discuss in Sect. 2.3. Once this divergent part is factorised, the remaining two-parton process $eq \to eq$ is evaluated numerically and this collinear contribution yields always a $\gamma + (0+1)$-jet final state. In obtaining the collinear factor, terms of order $\mathcal{O}(y_{\min})$ have been neglected so that to obtain reliable results, $y_{\min}$ is chosen to be small enough. For our numerical results below, we shall use $y_{\min} = 10^{-7}$.

The finite contribution, where the quark and the photon are theoretically separated is a three-parton process and is evaluated numerically for the three-parton phase space restricted by $y_{q\gamma} > y_{\min}$. The jet algorithm is then applied to retain only $\gamma + (0+1)$ jet final states. The $y_{\min}$ dependence in the finite and collinear contributions cancels numerically when those are added together, such that the total $\gamma + (0+1)$-jet cross section is independent of this slicing parameter $y_{\min}$. This independence yields an important check on the correctness of our calculation.

2.3 Fragmentation contributions

In addition to the production of hard photons in the final state, photons can also be produced through the fragmentation of a hadronic quark jet into a single photon carrying a large fraction z of the jet energy [1]. This fragmentation process is described in terms of the quark-to-photon fragmentation function, $D_{q\to\gamma}$, which is convoluted with the cross section for the electron-quark scattering process

$$l(p_1) + q(p_2) \to l(p_4) + q(p_{35})\,,$$

such that the final state photon and quark momenta are given by $p_3 = z p_{35}$ and $p_5 = (1-z)p_{35}$.

The fragmentation contribution to the $\gamma + (0+1)$-jet cross section associated with this fragmentation process is displayed in Fig. 2. It takes formally the following factorised form:

$$\int \mathrm{d}PS_2\, |M|^2_{lq\to lq} D_{q\to\gamma}(z)\, J^{(2)}_{\gamma+(0+1)}(p_{35}, p_r)\, \Theta(p_3, p_4)\,. \tag{3}$$

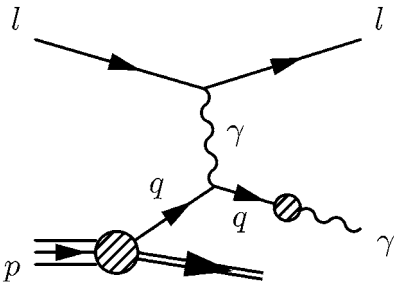

Fig. 2. Leading order Feynman amplitude for the quark-to-photon fragmentation process in deep inelastic scattering

Here $J^{(2)}_{\gamma+(0+1)}$, the jet function defining how to obtain $\gamma + (0+1)$ jets out of one parton and the proton remnant, is simply $\Theta(z > z_{\mathrm{cut}})$, and thus independent of the jet recombination procedure.

Like the hard photon contribution related to the parton process $lq \to lq\gamma$, this fragmentation contribution is of order α^3: The process $eq \to eq$ is of order α^2 while the quark-to-photon fragmentation function $D_{q\to\gamma}$ is of order α. The latter is given by,

$$D_{q\to\gamma}(z) = D_{q\to\gamma}(z, \mu_{\mathrm{F},\gamma}) + \frac{\alpha e_q^2}{2\pi} \times \left(P^{(0)}_{q\gamma}(z) \ln \frac{z(1-z) y_{\min} s_{lq}}{\mu^2_{\mathrm{F},\gamma}} + z \right). \tag{4}$$

Here $D_{q\to\gamma}(z, \mu_{\mathrm{F},\gamma})$ stands for the non-perturbative quark-to-photon fragmentation function describing the transition $q \to \gamma$ at the factorisation scale $\mu_{\mathrm{F},\gamma}$. Parametrizations for this function will be specified below. The second term in (4), if substituted in (3), represents the finite part obtained after absorption of the collinear quark–photon factor described in Sect. 2.2 into the bare fragmentation function as explained in [7].

In (4), $P^{(0)}_{q\gamma}$ is the LO quark-to-photon splitting function

$$P^{(0)}_{q\gamma}(z) = \frac{1 + (1-z)^2}{z} \tag{5}$$

and e_q is the electric charge of the quark q. The variable z denotes the fraction of the quark energy carried away by the photon, while s_{lq} is the lepton–quark squared centre-of-mass energy.

In order to turn the expression (3) into a cross section, one needs to know the non-perturbative quark-to-photon fragmentation function at the factorisation scale $\mu_{\mathrm{F},\gamma}$, $D_{q\to\gamma}(z, \mu_{\mathrm{F},\gamma})$. This function satisfies an evolution equation which determines its variation with respect to the factorisation scale $\mu_{\mathrm{F},\gamma}$ to all orders in α_{s}. Restricting ourselves to the zeroth order in α_{s}, at order α, this fragmentation function obeys the leading order evolution equation,

$$\frac{\mathrm{d}D_{q\to\gamma}(z, \mu_{\mathrm{F},\gamma})}{\mathrm{d}\ln\mu^2_{\mathrm{F},\gamma}} = \frac{\alpha e_q^2}{2\pi} P^{(0)}_{q\gamma}(z)\,. \tag{6}$$

The fixed-order exact solution at $\mathcal{O}(\alpha)$ then reads

$$D_{q\to\gamma}(z,\mu_{\mathrm{F},\gamma}) = \frac{\alpha e_q^2}{2\pi} P_{q\gamma}^{(0)}(z) \ln\left(\frac{\mu_{\mathrm{F},\gamma}^2}{\mu_0^2}\right) + D_{q\to\gamma}(z,\mu_0) \tag{7}$$

$D_{q\to\gamma}(z,\mu_0)$ is the quark-to-photon fragmentation function at some initial scale μ_0. This function and the initial scale μ_0 cannot be calculated and have to be determined from experimental data. First indications for a non-vanishing $D_{q\to\gamma}(z,\mu_0)$ could be obtained by the EMC Collaboration [29] from the study of photon spectra in deep inelastic scattering, which were however insufficient for a detailed measurement. The first determination of $D_{q\to\gamma}(z,\mu_0)$ was performed by the ALEPH Collaboration [8]. From their fit to the $e^+e^-\to\gamma+1$-jet data they obtained

$$D_{q\to\gamma}(z,\mu_0) = \frac{\alpha e_q^2}{2\pi}\left(-P_{q\gamma}^{(0)}(z)\ln(1-z)^2 - 13.26\right), \tag{8}$$

with $\mu_0 = 0.14\,\mathrm{GeV}$. We note that (7) is an exact solution of (6) at $\mathcal{O}(\alpha)$. Furthermore when we substitute the solution (7) into (4) the cross section becomes independent of the factorisation scale $\mu_{\mathrm{F},\gamma}$. This means that for the cancellation of the $\mu_{\mathrm{F},\gamma}$ dependence only the LO photon FF is needed. Nonetheless, in order to see the influence of the NLO corrections to $D_{q\to\gamma}(z,\mu_{\mathrm{F},\gamma})$, we shall also evaluate the $\gamma+(0+1)$-jet cross section in DIS with the inclusion of the NLO photon FF.

Similar to (7) the NLO fragmentation function $D_{q\to\gamma}(z,\mu_{\mathrm{F},\gamma})$ is obtained as the solution of the evolution equation, but now with $\mathrm{O}(\alpha\alpha_\mathrm{s})$ terms added on the right-hand side of (6):

$$\begin{aligned}\frac{\mathrm{d}D_{q\to\gamma}(z,\mu_{\mathrm{F},\gamma})}{\mathrm{d}\ln\mu_{\mathrm{F},\gamma}^2} &= \frac{\alpha e_q^2}{2\pi}\left[P_{q\gamma}^{(0)}(z) + \frac{\alpha_\mathrm{s}}{2\pi}C_\mathrm{F}P_{q\gamma}^{(1)}(z)\right] \\ &\quad + \frac{\alpha_\mathrm{s}}{2\pi}C_\mathrm{F}P_{qq}^{(0)}(z)\otimes D_{q\to\gamma}(z,\mu_{\mathrm{F},\gamma})\,.\end{aligned} \tag{9}$$

The resulting quark-to-photon FF at scale $\mu_{\mathrm{F},\gamma}$ is

$$\begin{aligned}D_{q\to\gamma}(z,\mu_{\mathrm{F},\gamma}) &= \frac{\alpha e_q^2}{2\pi}\left[P_{q\gamma}^{(0)}(z) + \frac{\alpha_\mathrm{s}}{2\pi}C_\mathrm{F}P_{q\gamma}^{(1)}(z)\right]\ln\left(\frac{\mu_{\mathrm{F},\gamma}^2}{\mu_0^2}\right) \\ &\quad + \frac{\alpha_\mathrm{s}}{2\pi}C_\mathrm{F}P_{qq}^{(0)}(z)\ln\left(\frac{\mu_{\mathrm{F},\gamma}^2}{\mu_0^2}\right) \\ &\quad \otimes\left[\frac{\alpha e_q^2}{2\pi}\frac{1}{2}P_{q\gamma}^{(0)}(z)\ln\left(\frac{\mu_{\mathrm{F},\gamma}^2}{\mu_0^2}\right)\right. \\ &\quad \left. + D_{q\to\gamma}(z,\mu_0)\right] + D_{q\to\gamma}(z,\mu_0)\,.\end{aligned} \tag{10}$$

$P_{q\gamma}^{(1)}(z)$ is the next-to-leading order quark-to-photon splitting function [30] and $P_{qq}^{(0)}(z)$ is the LO qq splitting function [2]. $D_{q\to\gamma}(z,\mu_0)$ is the initial value of the NLO FF, which contains all unknown long-distance contributions. The result in (10) is an exact solution of the evolution equation up to $\mathrm{O}(\alpha\alpha_\mathrm{s})$. The NLO photon FF has equally been determined [10] using the ALEPH $e^+e^-\to\gamma+1$-jet data [8]. A three parameter fit with $\alpha_\mathrm{s}(M_Z^2) = 0.124$ yielded

$$\begin{aligned}D_{q\to\gamma}^{\mathrm{NLO}}(z,\mu_0) = \frac{\alpha e_q^2}{2\pi}\big(&-P_{q\gamma}^{(0)}(z)\ln(1-z)^2 \\ &+ 20.8(1-z) - 11.07\big)\end{aligned} \tag{11}$$

with $\mu_0 = 0.64\,\mathrm{GeV}$. Inside the experimental errors this fit for the photon FF at μ_0 describes [10] the ALEPH data at least as good as the LO fit (8).

It should be noted that the above LO and NLO quark-to-photon FF do not take into account the resummation of powers of $\ln(\mu_{\mathrm{F},\gamma}^2/\mu_0^2)$ as conventionally implemented, e.g. via the Altarelli–Parisi evolution equations [2]. Such resummations are only unambiguous if the resummed logarithm is the only large logarithm in the kinematical region under consideration. If logarithms of different arguments can become simultaneously large, the resummation of one of these logarithms at a given order implies that all other potentially large logarithms are shifted into a higher order of the perturbative expansion, i.e. are neglected. In the evaluation of the $\gamma+1$-jet rate at $\mathcal{O}(\alpha)$ [8] and $\mathcal{O}(\alpha\alpha_\mathrm{s})$ [9] at LEP for $0.7 < z < 1$, one encounters at least two different potentially large logarithms, $\ln\mu_{\mathrm{F},\gamma}^2$ and $\ln(1-z)$. In the high-z region, where the photon is isolated or almost isolated, it is by far not clear that $\ln\mu_{\mathrm{F},\gamma}^2$ is the largest logarithm. Choosing not to resum the logarithms of $\ln\mu_{\mathrm{F},\gamma}^2$ is therefore equally justified for the case of large z, $z\to 1$.

In the conventional approach, powers of $\ln(\mu_{\mathrm{F},\gamma}^2/\mu_0^2)$ are resummed. The parton-to-photon FF's $D_{i\to\gamma}(z,\mu_{\mathrm{F},\gamma})$ then satisfy a system of inhomogeneous evolution equations [2]. The solution of these equations resums all leading logarithms of the type $\alpha_\mathrm{s}^n\ln^{n+1}\mu_{\mathrm{F},\gamma}^2$. Including $\mathcal{O}(\alpha_\mathrm{s})$ corrections to the splitting functions yields resummation of subleading logarithms of the type $\alpha_\mathrm{s}^n\ln^n\mu_{\mathrm{F},\gamma}^2$. Several parametrisations of the photon FF are available in this approach. These use some model assumptions to describe the initial FF at some low scale μ_0. The most recent parametrisation of the photon FF in this approach are the BFG fragmentation functions [6]. This parametrisation has been compared to the ALEPH $\gamma+1$-jet cross section which is sensitive to the large z region ($0.7 < z < 1$) and found to be in agreement with the data [11]. Previous parametrisations were proposed in [4, 5]. Those tend to predict the $\gamma+1$-jet cross section in excess compared to the ALEPH data and will not be considered in the remainder of this paper.

As already mentioned, the inclusion of the NLO quark-to-photon fragmentation function in our evaluation of the $\gamma+(0+1)$-jet cross section is not required to cancel the factorisation scale dependence of the cross section. There, only the leading order (LO) fragmentation function is required. However, the NLO quark-to-photon fragmentation function corresponds to an expansion in α_s of the resummed quark-to-photon fragmentation function derived in a conventional approach [11], neglecting the initial fragmentation function $D_{q\to\gamma}(z,\mu_0)$. It is therefore instructive to implement the NLO quark-to-photon fragmenta-

tion function in the evaluation of the observable. Doing so will enable us to compare the results obtained in different approaches.

Thus we have three different quark-to-photon FF at our disposal which have been compared and found to be in agreement with the ALEPH data: the fixed order LO parametrisation, using the ALEPH data directly to determine the initial distribution given in (7) and (8), a NLO determined function given by (10) and (11) directly fitted to the ALEPH data, and the NLO parametrisation of BFG. A detailed comparison of the two approaches (fixed order and conventional) is given in [11]. Results for the $\gamma+$ 1-jet rate for LEP as measured by ALEPH with these different parametrizations of the photon FF are also shown in [11]. Furthermore, results for the theoretical calculation of the $\gamma+(1+1)$-jet cross sections in DIS using those various fragmentation functions are discussed in [31].

In the remainder of this paper, we shall use these three parametrisations of the photon FF to predict differential $\gamma+(0+1)$-jet cross sections in DIS. Finally, for the numerical results presented in the following, we shall always use $\mu_{\mathrm{F},\gamma}^2 = Q^2$.

2.4 Numerical implementation

The $\gamma+(0+1)$-jet cross section involves two partonic contributions: the hard-photon production and quark-to-photon fragmentation processes. Consequently, the cross section which is evaluated numerically in the form of a parton-level Monte Carlo generator contains a three-parton channel and a two-parton channel. The three-parton channel is evaluated with the restriction that the quark and the photon are theoretically resolved, i.e. not collinear, defined by $y_{q\gamma} > y_{\min}$. A recombination algorithm yielding a $\gamma+(0+1)$-jet final state is then applied to the partons present in the final state and a $\gamma+(0+1)$-jet event is obtained as an event with a photon-jet and the proton remnant jet. The two-parton channel is proportional to the quark-to-photon fragmentation function and contains the contribution from collinear quark–photon radiation, in the region $y_{q\gamma} \leq y_{\min}$. In this case, the final state partons always build a $\gamma+(0+1)$-jet event. The partonic cross section for $\gamma+(0+1)$-jet production reads

$$\begin{aligned}\hat{\sigma} = &\int_{y_{q\gamma}>y_{\min}} \mathrm{d}PS_3\, |M|^2_{lq\to lq\gamma}\, J^{(3)}_{\gamma+(0+1)}(p_3,p_5,p_r) \\ &\times \Theta(p_3,p_4) + \int \mathrm{d}PS_2\, |M|^2_{lq\to lq} \\ &\times D_{q\to\gamma}(z)\, J^{(2)}_{\gamma+(0+1)}(p_{35},p_r)\,\Theta(p_3,p_4)\,. \end{aligned} \tag{12}$$

Contributions where the photon builds a jet on his own are also included in the first term of the above equation. These contributions are obtained if the quark is combined with the remnant or is at too low transverse momentum or at too large rapidity to be identified as a jet. The application of kinematical cuts on the outgoing electron and photon is formally given by $\Theta(p_3,p_4)$. Details concerning the jet function and the kinematical cuts will be given in Sect. 3.

Finally, the cross section σ for deep inelastic electron–proton scattering is obtained by a convolution between the parton-level cross section $\hat{\sigma}$ for a given quark flavour (12) with the corresponding parton distribution function summed over all quark and antiquark flavours. For this, we use the CTEQ6L [32] leading order parametrisation of parton distributions.

3 The $\gamma+(0+1)$-jet cross section

In this section, we present our predictions for the $\gamma+(0+1)$ jet cross section in DIS at leading order, i.e. to $\mathcal{O}(\alpha^3)$. We focus in particular on the photon energy distribution of the photon jet by studying differential distributions in the photon energy fraction z. An experimental photon identification appears to be realistic only for large z: $0.7 < z < 1$. By comparing the predictions obtained with different parametrisations of the quark-to-photon fragmentation function, we will demonstrate the sensitivity of this observable on the photon FF. From the measured differential cross section, these predictions could lead to a new determination of the quark-to-photon fragmentation function in DIS.

We recall that a measurement of the photon FF in DIS from the z-distribution of the $\gamma+(1+1)$-jet cross section was suggested in [31]. Compared to this, the measurement from the $\gamma+(0+1)$-jet cross section discussed here has an important advantage. The photon fragmentation function enters here already at the leading order, while it enters as a higher-order correction to the $\gamma+(1+1)$-jet cross section. Consequently, the ratio of the $z > 0.9$ contribution to the $0.7 < z < 0.9$ contributions is considerably larger in $\gamma+(1+1)$-jet final states than in $\gamma+(0+1)$-jet final states, which in turn renders the experimental separation of the different bins more difficult.

Before we present our results, we specify the kinematical selection criteria appropriate for the HERA experimental environment and give a brief description of the different jet algorithms used in our study.

3.1 Kinematical selection criteria

The results for the differential $\gamma+(0+1)$-jet cross section are obtained for energies and kinematical cuts appropriate for the HERA experiments [33]. A combined data sample of incoming positrons and electrons is considered here, with a positron fraction of 85.6%. The energies of the incoming electron (or positron) and proton are $E_e = 27.5\,\mathrm{GeV}$ and $E_p = 920\,\mathrm{GeV}$, respectively. The cuts on the DIS variables are chosen as follows:

$$\begin{aligned} &E_e > 10\,\mathrm{GeV}\,, \quad 151^\circ < \Theta_e < 177^\circ\,, \\ &Q^2 > 4\,\mathrm{GeV}^2 \quad \text{and} \quad y > 0.15\,. \end{aligned} \tag{13}$$

The cuts on the electron energy and the scattering angle are due to experimental requirements for the unambiguous identification of the electron, reflecting the geometry of the H1 detector. The cut on Q^2 is intended to ensure

deep inelastic scattering events, as opposed to photoproduction. As discussed earlier, this cut is effective on the parton level only for the QQ subprocess, while the LL subprocess can involve much lower virtualities of the exchanged photon. Deep inelastic scattering kinematics in the LL process are ensured experimentally by requiring multiple hadronic tracks in the final state, which we implemented by requiring a maximum rapidity of the outgoing quark $\eta_q < 3$. Finally, a cut on the energy transfer variable y is part of the preselection of deep inelastic events, intended to minimise effects of electromagnetic radiative corrections. In our study, we choose the minimal value of y considerably larger than in typical analyses in DIS: for the $\gamma + (0+1)$-jet final states this large minimum value of y enhances the importance of the fragmentation contribution relative to the hard photon radiation.

Final states are classified as $\gamma + (0+1)$-jet events after a jet algorithm has been applied to the momenta of the final state hadrons and the photon. The photon is treated like the quark during the jet formation according to the so-called democratic procedure [7]. If a jet is formed, it is called "photon-jet" if the photon carries a large fraction of the jet energy (or jet transverse energy) $z > z_{\rm cut}$.

For this observable, it is crucial to apply the jet algorithm in the HERA laboratory frame. This situation is different from most studies of $(n+1)$-jet production in DIS ($n \geq 2$), which are preferably performed in the γ^*–proton centre-of-mass frame. In these studies, the positive z-axis is chosen to be the proton direction, proton and virtual photon are back-to-back and the produced hard jets are also back-to-back in transverse momentum. This is also the situation one faces when examining the production of $\gamma + (1+1)$ jets as described in [31]. In this case, the transverse energy of the photon-jet is balanced against the transverse energy of the other hard jet in the final state.

However in the evaluation of the $\gamma + (0+1)$-jet production at leading order, there is no hard jet to be back-to-back to the photon-jet. Indeed, if one views this observable in the γ^*–proton centre-of-mass frame, the quark–photon system is back-scattered in the negative z-direction. Final state photon and quark are therefore at vanishing transverse momentum, and a photon jet cannot be defined in a sensible manner in this frame.

In the HERA laboratory frame on the other hand, incoming proton and electron as well as the proton remnant move along the z-axis (with positive z-direction defined by the incoming proton). The photon-jet has a transverse momentum with respect to this axis, which is counterbalanced by the transverse momentum of the outgoing electron. In this frame, jets are constructed using one of the jet algorithms explained below and described by their rapidity η_j and transverse energy $E_{{\rm T},j}$ in the HERA frame. The rapidity of the photon jet $\eta_{\gamma-{\rm jet}}$ is also called photon rapidity η_γ. One defines the photon energy fraction inside the photon-jet by

$$z = \frac{E_{{\rm T},\gamma}}{E_{{\rm T},\gamma-{\rm jet}}}\,. \tag{14}$$

On the level of the theoretical calculation an analoguous jet algorithm is applied to cluster the final state quark, photon and proton remnant into $\gamma + (0+1)$-jet final states. If photon and quark are clustered together to form the photon jet, we have the corresponding theoretical expression for the photon energy fraction inside the photon-quark cluster given by,

$$z = \frac{E_{{\rm T},\gamma}}{E_{{\rm T},\gamma} + E_{{\rm T},q}}\,. \tag{15}$$

While for photon and quark not being merged in the same jet, we always find $z = 1$.

For our predictions we use $z_{\rm cut} = 0.7$ to identify a jet as photon jet. Furthermore, cuts are imposed on the photon-jet itself. The photon-jet is required to have a minimum transverse energy in the HERA frame, $E_{{\rm T},\gamma-{\rm jet}} > 3\,{\rm GeV}$ and its rapidity is restricted to be $-1.2 < \eta_{\gamma-{\rm jet}} < 1.8$. If photon and quark are not combined into a single jet, and the quark is also not combined with the proton remnant, we expect to have a $\gamma + (1+1)$-jet final state. However, this final state is observed only if the quark jet can be identified, i.e. has sufficient transverse energy $E_{{\rm T},q} > 2.5\,{\rm GeV}$ and is inside the detector coverage ($-2.1 < \eta_q < 2.1$). If the quark is forming a jet on its own outside these quark jet cuts, one still observes $\gamma + (0+1)$-jet final states.

3.2 Jet algorithms

Concerning the jet formation itself, two kinds of jet algorithms are commonly used to study jet production in DIS [34, 35]: the hadronic $k_{\rm T}$-algorithm [36], which was developed originally for hadron colliders, and a modified version of the Durham $k_{\rm T}$-algorithm [37], adapted for deep inelastic scattering [38]. We briefly describe each algorithm in this section.

In the hadronic $k_{\rm T}$-algorithm, which is applied here in the HERA laboratory frame, one computes for each particle i and for each pair of particles i, j the quantities

$$\begin{aligned} d_i &= E_{{\rm T},i}^2\,, \\ d_{ij} &= \min\left(E_{{\rm T},i}^2, E_{{\rm T},j}^2\right)\left((\eta_i-\eta_j)^2 + (\phi_i-\phi_j)^2\right)/R^2\,, \end{aligned} \tag{16}$$

where η_i is the rapidity of particle i and ϕ_i is its polar angle in the plane perpendicular to the incoming beam direction. R is the jet resolution parameter in this algorithm. One then searches the smallest of all d_i and d_{ij}, which is labeled $d_{\rm min}$. If $d_{\rm min}$ is a d_i, then particle i is identified as a jet and removed from the clustering procedure. If $d_{\rm min}$ is a d_{ij}, particles i, j are merged into a new particle (proto-jet) with

$$\begin{aligned} E_{{\rm T},ij} &= E_{{\rm T},i} + E_{{\rm T},j}\,, \quad \eta_{ij} = \frac{E_{{\rm T},i}\eta_i + E_{{\rm T},j}\eta_j}{E_{{\rm T},ij}}\,, \\ \phi_{ij} &= \frac{E_{{\rm T},i}\phi_i + E_{{\rm T},j}\phi_j}{E_{{\rm T},ij}}\,. \end{aligned} \tag{17}$$

The algorithm is repeated until all remaining particles or proto-jets are identified as jets. Experimentally observable

jets are then required to have some minimal amount of transverse energy $E_{\mathrm{T,min}}$. All jets below $E_{\mathrm{T,min}}$ are unobservable (and can thus be considered part of the proton remnant); the resolution parameter R does therefore control how likely a low energy particle is clustered into the harder jets or into the remnant.

Applied on the parton level, one computes

$$d_{\gamma q} = \min\left(E^2_{\mathrm{T},\gamma}, E^2_{\mathrm{T},q}\right)\left((\eta_\gamma - \eta_q)^2 + (\phi_\gamma - \phi_q)^2\right)/R^2 \tag{18}$$

and recombines photon and quark if

$$d_{\gamma q} < \min\left(E^2_{\mathrm{T},\gamma}, E^2_{\mathrm{T},q}\right) . \tag{19}$$

This condition can be expressed purely in terms of the angular distance of photon and quark:

$$(\eta_\gamma - \eta_q)^2 + (\phi_\gamma - \phi_q)^2 < R^2 . \tag{20}$$

It should be noted that this simplified condition is valid only at the leading order, where the hadronic k_{T}-algorithm is applied only to two partons (quark and photon) and thus performs only a single iteration. As soon as more than two partons are present (at higher orders), the algorithm iterates over all possible pairs of partons. It is noteworthy that (20) is identical to the recombination condition which is used in the cone algorithm [13] in jet studies at hadron colliders and also in cone-based definitions of isolated photons. In these, the resolution parameter R is the cone size. A detailed comparison of the hadronic k_{T}-algorithm and the cone algorithm can be found in [36].

If condition (19) is fulfilled, quark and photon are recombined into a single photon jet at parton level, which has

$$E_{\mathrm{T},\gamma-\mathrm{jet}} = E_{\mathrm{T},\gamma} + E_{\mathrm{T},q} , \qquad \eta_{\gamma-\mathrm{jet}} = \frac{E_{\mathrm{T},\gamma}\eta_\gamma + E_{\mathrm{T},q}\eta_q}{E_{\mathrm{T},\gamma-\mathrm{jet}}} . \tag{21}$$

The modified Durham k_{T}-algorithm [38], also applied in the HERA laboratory frame and adapted to the application in DIS features an important difference to the original formulation for e^+e^- annihilation: the proton remnant is taken into account in the jet formation. For this algorithm, we consider the exclusive and inclusive formulation: the inclusive k_{T}-algorithm clusters until only the desired $\gamma + (0+1)$-jet final state is left, while the exclusive k_{T}-algorithm stops the recombination of particles according to a jet resolution parameter. A detailed discussion of both options for jet production in DIS can be found in [34, 35].

Both inclusive and exclusive k_{T}-algorithms applied in the HERA laboratory frame calculate the quantity

$$E^2_{\mathrm{T},ij} = 2\min\left(E^2_{\mathrm{T},i}, E^2_{\mathrm{T},j}\right)(1 - \cos\theta_{ij}) \tag{22}$$

for each pair i, j of particles. The pair with the lowest $E^2_{\mathrm{T},ij}$ is then combined into a new particle by adding the momenta of i and j. For the inclusive k_{T}-algorithm, this procedure is repeated until only a $\gamma + (0+1)$ jet final state is left, while for the exclusive k_{T}-algorithm, the procedure stops as soon as the pair with the lowest $E^2_{\mathrm{T},ij}$ has $E^2_{\mathrm{T},ij}/W^2 < y_{\mathrm{cut}}$, where W^2 is the total invariant mass of the hadronic final state including the photon. y_{cut} is the experimental jet resolution parameter, it determines the broadness of the jet. It has in fact a similar role as R, the resolution parameter of the hadronic k_{T}-algorithm, or the radius of the cone in the cone algorithm.

On the parton level, we compute (22) for i, j being each pair of two of the three partons: photon, quark and proton remnant. The jet algorithm then selects the minimum of these three quantities. In the inclusive case, the pair i, j of partons with the minimal value of $E^2_{\mathrm{T},ij}$ is always combined, while for the exclusive case this pair is combined only if $E^2_{\mathrm{T},ij}/W^2 < y_{\mathrm{cut}}$ with W^2 being the squared invariant mass of photon, quark and proton remnant.

Quark and photon build one jet if the minimal value of $E^2_{\mathrm{T},ij}$ is given by $E^2_{\mathrm{T},\gamma q}$ (in the exclusive case, $E^2_{\mathrm{T},\gamma q}/W^2 < y_{\mathrm{cut}}$ has to be fulfilled as well). If photon and remnant are combined, the event is always discarded, while it is always accepted if quark and remnant are combined. In this case, the photon forms a jet on its own. In the exclusive case, we can have photon, quark and remnant forming each a jet on their own, i.e. yielding a $\gamma + (1+1)$-jet final state. As we will see, for large values of y_{cut} (above $y_{\mathrm{cut}} = 0.1$) both inclusive and exclusive jet algorithms lead to very similar predictions for the $\gamma + (0+1)$-jet cross section.

If photon and quark are combined, we compute for the photon jet

$$E_{\mathrm{T},\gamma-\mathrm{jet}} = E_{\mathrm{T},\gamma} + E_{\mathrm{T},q} , \qquad \eta_{\gamma-\mathrm{jet}} = \frac{1}{2}\log\frac{E_\gamma + E_q + p_{z,\gamma} + p_{z,q}}{E_\gamma + E_q - p_{z,\gamma} - p_{z,q}} . \tag{23}$$

We finally recall that applying any of the jet algorithms on the parton level will classify two types of partonic contributions as $\gamma + (0+1)$-jet final states. Events where the quark and photon are recombined into a jet will have $z < 1$. On the other hand events where the photon forms a jet on its own while the quark is combined with the remnant or is produced at too low transverse energy or too large rapidity to be observed as a jet are also identified as $\gamma + (0+1)$-jet, with $z = 1$.

3.3 Measuring the quark-to-photon fragmentation function

Predictions for the $\gamma + (0+1)$-jet cross section differential in z, obtained using the kinematical cuts specified in Sect. 3.1 and defined using the jet algorithms in the laboratory frame, are displayed in Fig. 3. We use the three different parametrisations of the photon fragmentation functions discussed in Sect. 2.3 and apply either the inclusive or exclusive k_{T}-algorithm for different values of the resolution parameter y_{cut}. Results are given as bin-integrated cross sections for three bins, as anticipated [33] for the experimental measurement.

Concerning the variation with the jet resolution parameter, we observe that the inclusive k_{T}-algorithm and the

exclusive k_T-algorithm for large $y_{cut} = 0.1$ and above yield very similar results, indicating that for large y_{cut}, practically all events are classified as $\gamma + (0+1)$ jet. A visible variation of the cross section is observed only at much lower y_{cut}, $y_{cut} \ll 0.01$. For $y_{cut} = 0.004$ and even more for $y_{cut} = 0.001$, we observe that the $z > 0.9$ contribution decreases considerably, while the contributions for lower z remain largely unmodified. This can be understood from the fact that with decreasing y_{cut}, particles are less likely to be recombined into jets. In our case, especially quark and remnant are combined less often, such that more events at $z = 1$ are classified as $\gamma + (1+1)$-jet events, resulting in a decrease of the $\gamma + (0+1)$-jet cross section in the last bin in z.

If we compare our results for the various photon FFs in Fig. 3, we observe that the predictions agree approximately within 5% in the large z region, i.e. for $z > 0.9$. However, near the minimum of the cross section, i.e. in the region $0.7 < z < 0.9$, the results differ considerably by up to a factor 2 in $0.7 < z < 0.8$ and up to a factor 5 in $0.8 < z < 0.9$. The largest differences occur between the predictions obtained with the LO ALEPH photon fragmentation function on the one hand and the BFG parametrisation on the other hand. This discrepancy comes mainly from the fact that different evolution approaches are used. Whereas for BFG the FF at $\mu^2_{F,\gamma} = Q^2$ is obtained from the conventional evolution resumming the leading and subleading logarithms of $\mu_{F,\gamma}$, the ALEPH photon FFs are evolved only to the respective finite order in α_s as given in (7) and (10). Therefore, if we calculated the $\gamma + (0+1)$-jet cross section at the large scale $\mu^2_{F,\gamma} = M_Z^2$ the cross sections obtained for BFG and ALEPH would come out quite similar over the whole z-range inside a 20% margin. Only when we go to the scale $\mu^2_{F,\gamma} = Q^2$, which is much smaller than M_Z^2, we observe that the cross section obtained using the BFG photon fragmentation function is much larger than the ALEPH cross section in the region $0.7 < z < 0.9$. This was already observed in [31] when comparing the predictions obtained for the $\gamma + (1+1)$-jet cross section in DIS.

Since the non-perturbative input distributions and higher order splitting functions contain explicit $\log(1-z)$ terms, it is however not clear if the resummed fragmentation functions can be considered to be reliable for $z > 0.95$ [11]. Provided the resummed solution of the evolution equation is accurate over the whole z-range under consideration, i.e. for $0.7 < z_\gamma < 1$, the approach using this solution represents the theoretically preferred one as it is the most complete. The fixed order approach using an expanded and therefore approximated photon FF has on the other hand also important advantages. As already

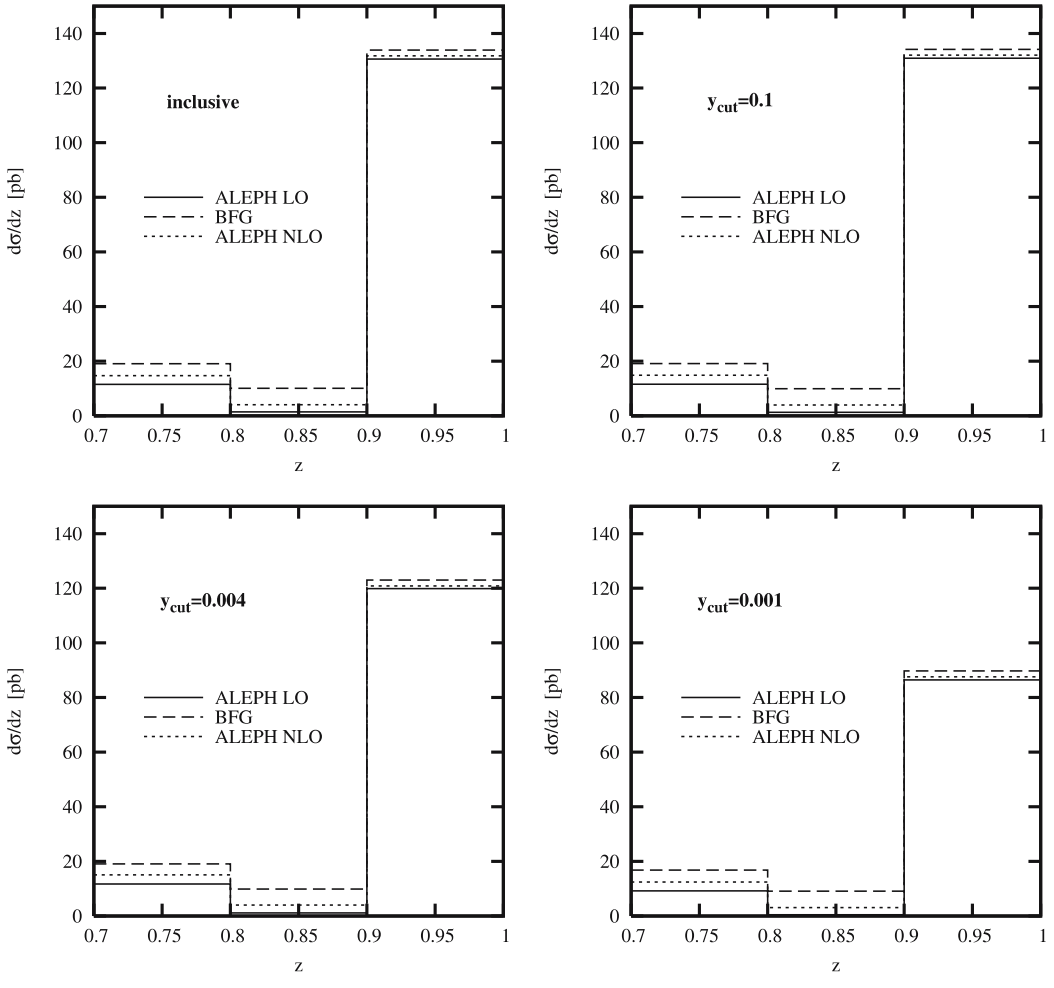

Fig. 3. Photon energy distribution inside the photon jet of $\gamma + (0+1)$-jet events. Jets are defined using the inclusive and exclusive k_T-algorithm. In the latter case the jet resolution parmeter y_{cut} is taken equal to 0.1, 0.004 and 0.001 respectively

mentioned, its use leads to factorisation scale independent results for the cross section evaluated at a given fixed order in α_s. Moreover it enables an analytic determination of the photon FF.

As the predictions for the $\gamma+(0+1)$-jet cross section obtained using different parametrisations differ considerably, this observable is highly sensitive on the photon FF and would be an appropriate observable to measure in view of extracting the quark-to-photon fragmentation function in DIS. Such a measurement could also be used to test the existing approaches to the FF discussed in Sect. 2.3.

Finally, using the hadronic k_T-algorithm, the fraction of events where photon and quark are clustered together is considerably smaller than the one obtained using the exclusive (or inclusive) k_T-algorithm in the laboratory frame. As a consequence, more events are in the last bin $z > 0.9$, and the fraction of events in the two other bins becomes negligible. Using either fragmentation function, one observes that, for the hadronic k_T-algorithm with separation parameters $R \leq 1$, negative contributions are predicted for the bins $0.7 < z < 0.8$ and $0.8 < z < 0.9$ for all fragmentation functions considered in this paper. These unphysical predictions can be understood as follows: one observes two types of logarithms in the z-distribution of the $\gamma+(0+1)$-jet cross section: $\ln(E_{T,\gamma}^2/Q^2)$ and $\ln(k_{T,\gamma-q}^2/Q^2)$, where $k_{T,\gamma-q}$ is the maximum transverse momentum of the quark and the photon with respect to the photon jet direction allowed by the jet algorithm. While the former logarithms do not become large, since $E_{T,\gamma}^2$ and Q^2 are typically of the same magnitude, the latter logarithms can become large, if the jet algorithm is too restrictive in recombining quark and photon. In the case of the hadronic k_T-algorithm, $k_{T,\gamma-q}^2$ becomes much smaller than typical hadronisation scales for large z, and either approach (fixed order or resummed) to the photon fragmentation function loses its applicability. For the ALEPH NLO and BFG parametrisations, this effect may be accounted for in part by lowering the factorisation scale $\mu_{F,\gamma}$ associated with the photon fragmentation process, but for large z, $k_{T,\gamma-q}^2$ in the hadronic k_T-algorithm is too low to be taken as $\mu_{F,\gamma}$. Therefore, a measurement of the photon fragmentation function from the $\gamma+(0+1)$-jet cross section should be based on the HERA-frame exclusive (or inclusive) k_T-algorithm, which admits larger values of $k_{T,\gamma-q}^2$, thus avoiding the appearance of the above-mentioned large logarithmic corrections.

4 The isolated $\gamma+(0+1)$-jet and inclusive γ cross sections

Production of isolated photons in association with hadrons has been widely studied in different collider environments. The measured isolated photon cross sections were used as tests of the hard interaction dynamics, or to measure auxiliary quantities such as parton distributions. A very sensitive issue is the definition of isolated photons produced in association with hadrons, since a completely isolated photon is not an infrared-safe observable in quantum chromodynamics (QCD). At present, this isolation is usually accomplished experimentally by admitting a limited amount of hadronic energy inside a cone around the photon direction.

The ZEUS study of isolated photon production in deep inelastic scattering [14] was carried out using such a cone-based isolation criterion, requiring the photon to carry at least 90% of the energy inside a cone of unit radius in rapidity and polar angle, thus admitting 10% of hadronic energy. We showed in [21] that the ZEUS measurement could be well reproduced in all its aspects by a parton-level calculation, closely related to the calculation of the $\gamma+(0+1)$-jet cross section described above. In fact, the isolated photon cross section can be obtained from (12) by replacing the n-particle jet functions $J_{\gamma+(0+1)}^{(n)}(p_3,p_5,p_r)$ by a photon isolation definition $I_\gamma^{(n)}(p_3,p_5)$. The cone-based isolation definition $I_\gamma^{(3)}(p_3,p_5)$ checks if the quark momentum p_5 is inside the cone defined by the photon momentum p_3, and subsequently applies a cut on the photon energy fraction $z > z_{cut}$. Since in the two-parton contribution, quark and photon momenta are always collinear, $I_\gamma^{(2)}(p_3,p_5)$ amounts simply to a cut on the photon energy fraction $z > z_{cut}$. The cross section for isolated photon production is thus also dependent on the photon fragmentation function. As demonstrated in [21], its prediction is however only marginally sensitive on the parametrisation used for the photon fragmentation function. In the following, we will therefore compute all predictions using just the ALEPH LO fragmentation function.

The cone-based isolation criterion has several conceptual drawbacks. The cone size cannot be chosen much smaller than unity [39], as often required for new particle searches, since a small cone size would spoil the convergence of the perturbative expansion for the isolated photon cross section. The interplay of the isolation cone with other kinematical cuts can also sometimes lead to a discontinuous behaviour of the cross section [40]. Also, when studying the production of photons in association with hadronic jets, the application of the cone-based photon isolation could become ambiguous, since it is not clear how to attribute the hadronic activity in the photon isolation cone to the jets.

To circumvent the problems of the cone-based photon isolation, several alternative photon isolation criteria were proposed in the literature. A dynamic cone-based isolation [12] could in principle allow one to eliminate the dependence on the photon fragmentation function; this was however not accomplished in an experimental measurement up to now. In the democratic clustering procedure proposed in [7], isolated photon cross sections are directly derived from jet cross sections. In this approach, which was already used to define the $\gamma+(0+1)$-jet cross section in Sect. 2.3, the jet algorithm treats the photon like any other hadron, resulting it to be clustered into one of the final state jets, which is then called the photon jet. An isolated photon in this approach is a photon jet where the photon carries more than a certain fraction of the jet energy. Using this democratic clustering approach, the ALEPH Collaboration measured the isolated $\gamma+1$-jet

rate [8] for the k_{T}-algorithm [37], using $z_{\mathrm{cut}} = 0.95$ to define isolated photons. Using the fragmentation function previously determined from the photon energy spectra of the $\gamma + 1$-jet rate [8], good agreement between experimental data and theory was found for a wide range of jet resolution parameters. This agreement improved considerably by including NLO corrections [9, 10].

In this section, we study isolated photon cross sections in DIS, obtained using different jet algorithms. In contrast to the discussion of the previous section, where we aimed to maximise the sensitivity of our observable on the photon fragmentation function by restrictive cuts and by choosing a specific jet algorithm, here we choose a less restraint event selection. As before, we assume a combined data sample of incoming positrons and electrons, with a positron fraction of 85.6%, with $E_e = 27.5\,\mathrm{GeV}$ and $E_p = 920\,\mathrm{GeV}$. Our choice of cuts is again motivated by the coverage of the H1 detector [33]. In particular, we apply the following cuts on the DIS variables:

$$E_e > 10\,\mathrm{GeV}\,, \quad 151^\circ < \Theta_e < 177^\circ\,,$$
$$Q^2 > 4\,\mathrm{GeV}^2 \quad \text{and} \quad y > 0.05\,. \tag{24}$$

Events selected using these criteria and containing a photon candidate are then processed using a jet algorithm. We have seen in the previous section that the difference between the inclusive and exclusive laboratory frame k_{T}-algorithm is only marginal, except for very small jet resolution parameters y_{cut}. For our studies here, we do therefore use only the exclusive laboratory frame k_{T}- algorithm with $y_{\mathrm{cut}} = 0.1$ and the hadronic k_{T}-algorithm with jet resolution parameter $R = 1$. Both jet algorithms result in final states containing a number of hard jets, with one of the jets containing the photon candidate. If the photon carries more than 90% of the transverse energy of this photon jet ($z_{\mathrm{cut}} = 0.9$), it is called isolated. We then apply cuts on the photon transverse energy $E_{\mathrm{T},\gamma}$ and the photon rapidity η_γ:

$$E_{\mathrm{T},\gamma} > 3\,\mathrm{GeV}\,, \qquad -1.2 < \eta_\gamma < 1.8\,. \tag{25}$$

Applying the jet algorithm, one obtains either $\gamma + (0+1)$-jet or $\gamma + (1+1)$-jet final states, with the quark forming a jet on its own in the latter case. As before, these are identified as $\gamma + (1+1)$-jet events only if the quark jet can be seen inside the detector coverage, i.e. if

$$E_{\mathrm{T},q} > 2.5\,\mathrm{GeV}\,, \qquad -2.1 < \eta_q < 2.1\,. \tag{26}$$

Using these cuts, we can define two different isolated photon cross sections: the isolated $\gamma + (0+1)$-jet cross section, which contains only events where no quark jet is observed, and the inclusive isolated γ cross section, where no restrictions are applied on the quark jet. Note that for the inclusive HERA-frame k_{T}-algorithm, these two cross sections would coincide exactly. As seen in the previous section, results obtained using the inclusive HERA-frame k_{T}-algorithm are almost identical to results obtained from

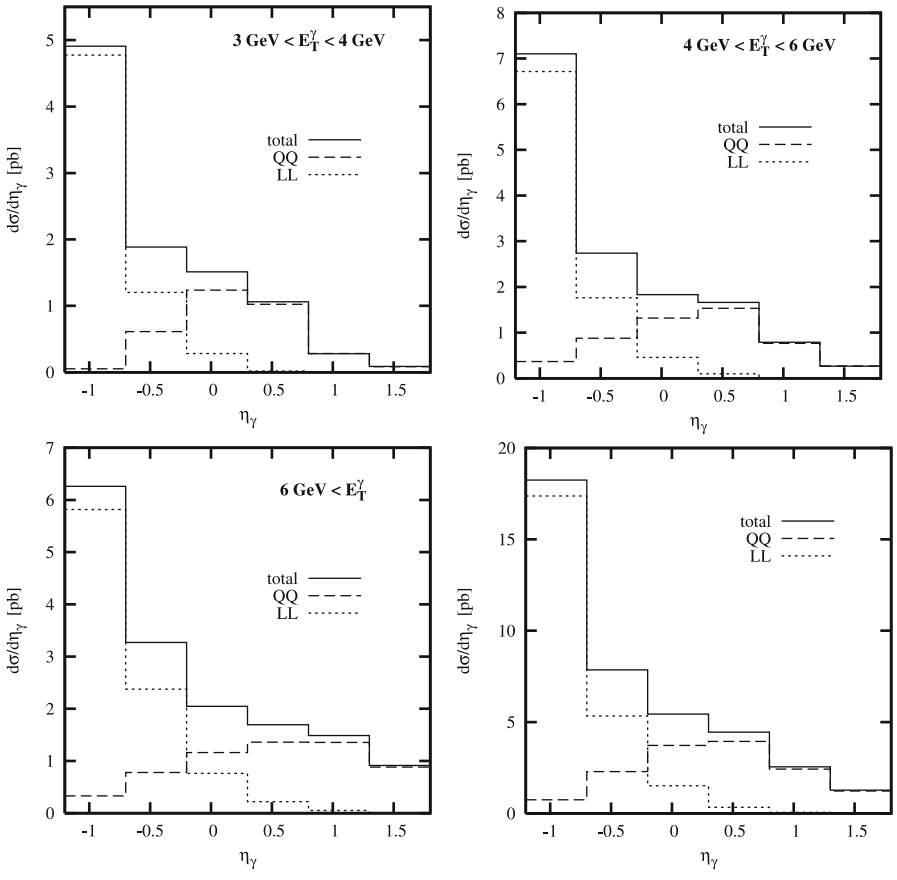

Fig. 4. Rapidity distributions of isolated photons in $\gamma + (0+1)$-jet events, in different bins in $E_{\mathrm{T},\gamma}$. The *last plot* shows the sum over all bins. Isolated photons are defined here using the exclusive k_{T}-algorithm ($y_{\mathrm{cut}} = 0.1$) in the HERA frame, requiring $z > 0.9$. *LL* and *QQ* subprocess contributions are indicated as *dashed* and *dotted lines*

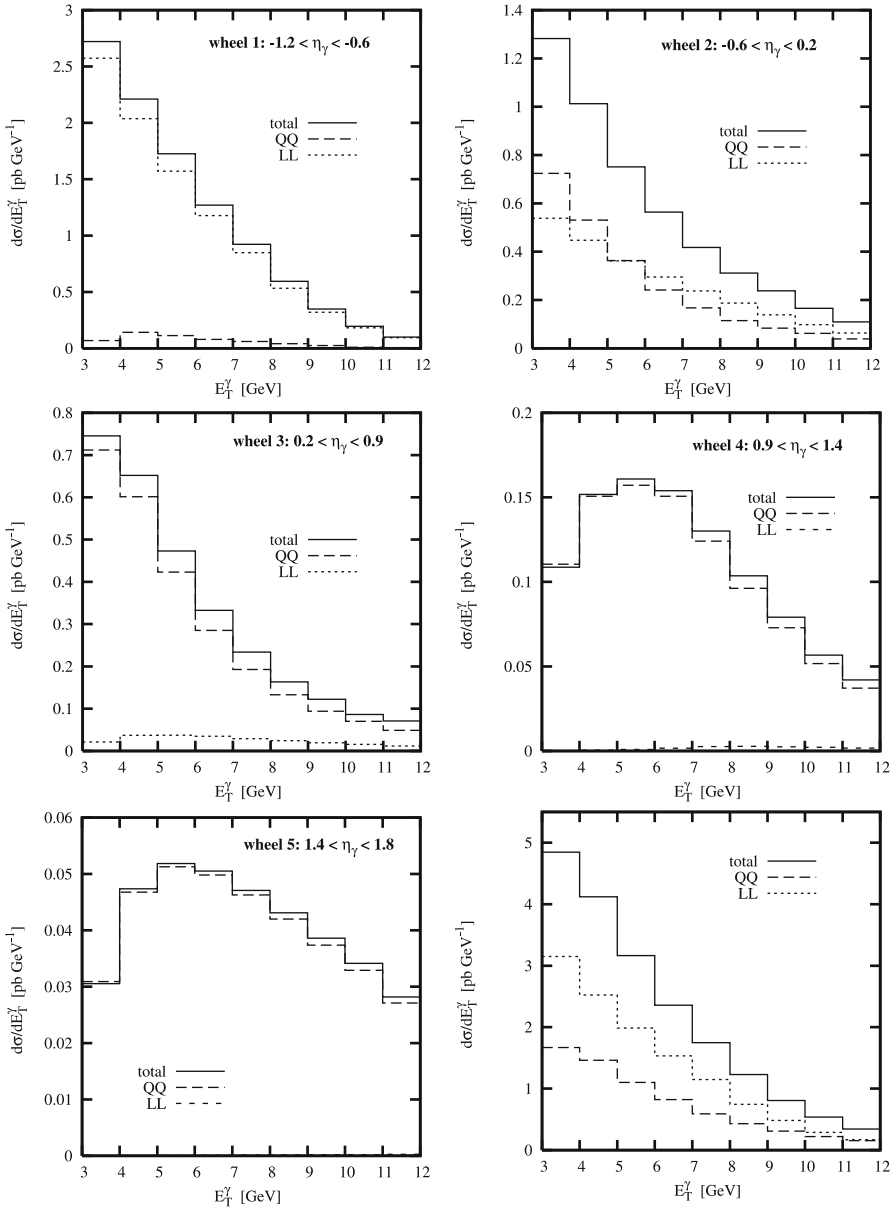

Fig. 5. Transverse energy distributions of isolated photons in $\gamma + (0+1)$-jet events, in different bins in η_γ. The *last plot* shows the sum over all bins. Isolated photons are defined using the exclusive k_T-algorithm ($y_\mathrm{cut} = 0.1$) in the HERA frame, requiring $z > 0.9$. LL and QQ subprocess contributions are indicated as *dashed* and *dotted lines*

the exclusive algorithm for $y_\mathrm{cut} = 0.1$, as applied here. Therefore, there is only very little difference between the isolated $\gamma + (0+1)$-jet cross section and the isolated inclusive γ cross section for this algorithm.

Figures 4 and 5 display the rapidity and transverse energy distributions of isolated photons in $\gamma + (0+1)$-jet events using the exclusive k_T-algorithm in the HERA-frame. QQ and LL contributions to these distributions are indicated separately, and the total is obtained by summing QQ, LL and QL contributions. The total $\gamma + (0+1)$-jet cross section with this jet algorithm and the above-mentioned cuts is 19.9 pb. For the rapidity distributions, we consider three different bins in transverse energy, displayed in Fig. 4. The rapidity distribution of photons in $\gamma + (0+1)$-jet production shows features similar to the rapidity distribution of inclusive isolated photons, discussed in [21]. The distributions resemble each other in all bins in $E_{\mathrm{T},\gamma}$, and fall towards increasing η_γ. The contributions of the QQ and LL subprocesses are of comparable magnitude, but have considerably different shapes in η_γ: the LL process is largest in the backward direction (i.e. in the direction of the outgoing electron) and falls rapidly towards positive η_γ, becoming negligible above $\eta_\gamma \gtrsim 0.5$. The shape of the LL process on one hand, differs very little for the different bins. The QQ process, on the other hand, is most pronounced at mid-rapidity, with a maximum around $\eta_\gamma \approx 0.5$ for the sum of all $E_{\mathrm{T},\gamma}$-bins. The position of this η_γ-maximum of the QQ process shifts from lower η_γ in the lowest $E_{\mathrm{T},\gamma}$-bin (where it is around $\eta_\gamma \approx 0$) to higher η_γ in the highest $E_{\mathrm{T},\gamma}$-bin (maximum around $\eta_\gamma \approx 1$). The three different bins are of increasing size, and contribute about equal amounts to the total η_γ-distribution.

The transverse energy distributions, Fig. 5, are considered in five different bins in η_γ, corresponding to five different wheels of the electromagnetic calorimeter of the H1 detector [33]. The numbering of the wheels is from

the backward towards the forward direction. In the first wheel ($-1.2 < \eta_\gamma < -0.6$), the cross section is completely dominated by the LL process, and falls monotonously with $E_{\mathrm{T},\gamma}$. Already in the second wheel ($-0.6 < \eta_\gamma < 0.2$), QQ and LL processes are of similar magnitude, and also of rather similar shape in $E_{\mathrm{T},\gamma}$. In the third wheel ($0.2 < \eta_\gamma < 0.9$) and beyond, the contribution from the LL process is negligible. Like in the first two wheels, the $E_{\mathrm{T},\gamma}$-distribution falls monotonously in the third wheel. In the fourth ($0.9 < \eta_\gamma < 1.4$) and fifth ($1.4 < \eta_\gamma < 1.8$) wheels, the $E_{\mathrm{T},\gamma}$-distribution is peaked around $E_{\mathrm{T},\gamma} \approx 5.5\,\mathrm{GeV}$. This feature is a consequence of the exclusive HERA-frame k_T-algorithm used here: photons produced at low transverse energy in the forward region are recombined with the proton remnant, and do therefore not contribute to the measured cross section. The total transverse energy distribution (summed over all wheels in rapidity) is dominated by the first three wheels, and thus receives similar contributions from the QQ and LL processes; as always the QL process is of negligible magnitude.

In Figs. 6 and 7 we show the rapidity and transverse energy distributions of isolated photons in $\gamma + (0+1)$-jet events using the hadronic k_T-algorithm ($R = 1$). As for the HERA-frame exclusive k_T-algorithm, QQ and LL contributions are indicated separately, and the total is obtained by summing QQ, LL and QL contributions. We also use the same bins as before. The total $\gamma + (0+1)$-jet cross section with the hadronic k_T-algorithm is 19.1 pb, which is very similar to the total cross section in the HERA-frame exclusive k_T-algorithm. Many features of the distributions are similar to what we observed above. In the discussion of these figures, we therefore only focus on differences arising from the use of the two different algorithms.

In the rapidity distributions, Fig. 6, we observe that the shape of the LL contribution is similar for both jet algorithms, while the QQ contribution looks considerably different. As opposed to Fig. 4, we see that the QQ subprocess remains sizable also in the backward rapidity region, especially at low $E_{\mathrm{T},\gamma}$.

The difference between the two jet algorithms is more pronounced in the transverse energy distribution, Fig. 7. With increasing $E_{\mathrm{T},\gamma}$, this distribution falls more steeply for the hadronic k_T-algorithm than for the HERA-frame exclusive k_T-algorithm. Also, one observes in the forward region (the fourth and fifth wheel) that photons at low transverse energy are not disfavoured as in Fig. 5, where they were combined with the proton remnant in a sizable fraction of the events. As a consequence, the total transverse energy distribution falls more steeply than for the HERA-frame exclusive k_T-algorithm.

As explained above, the exclusive k_T-algorithm in the HERA-frame almost always yields $\gamma + (0+1)$-jet final states, such that in this algorithm the isolated $\gamma + (0+1)$-jet cross section nearly coincides with the inclusive isolated γ cross section. In contrast, application of the hadronic k_T-algorithm results in $\gamma + (0+1)$-jet and $\gamma + (1+1)$-jet final states. At the leading order in perturbation theory used here, the inclusive isolated γ cross section in this

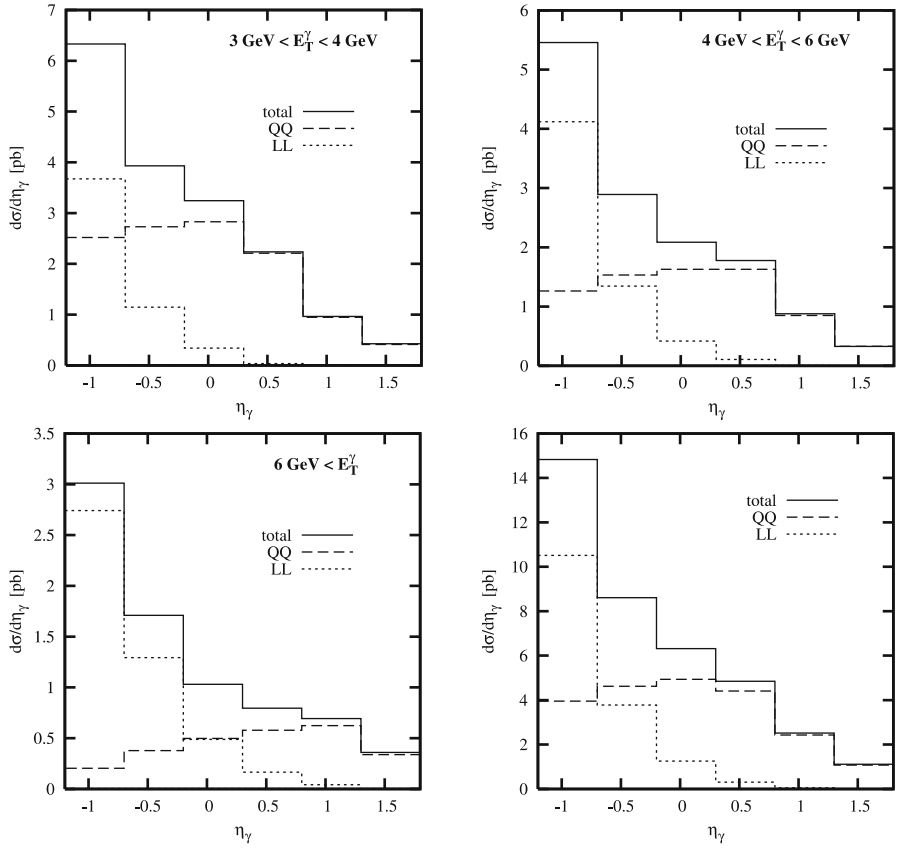

Fig. 6. Rapidity distributions of isolated photons in $\gamma + (0+1)$-jet events, in different bins in $E_{\mathrm{T},\gamma}$. The *last plot* shows the sum over all bins. Isolated photons are defined here using the hadronic k_T-algorithm ($R = 1$), requiring $z > 0.9$. LL and QQ subprocess contributions are indicated as *dashed* and *dotted lines*

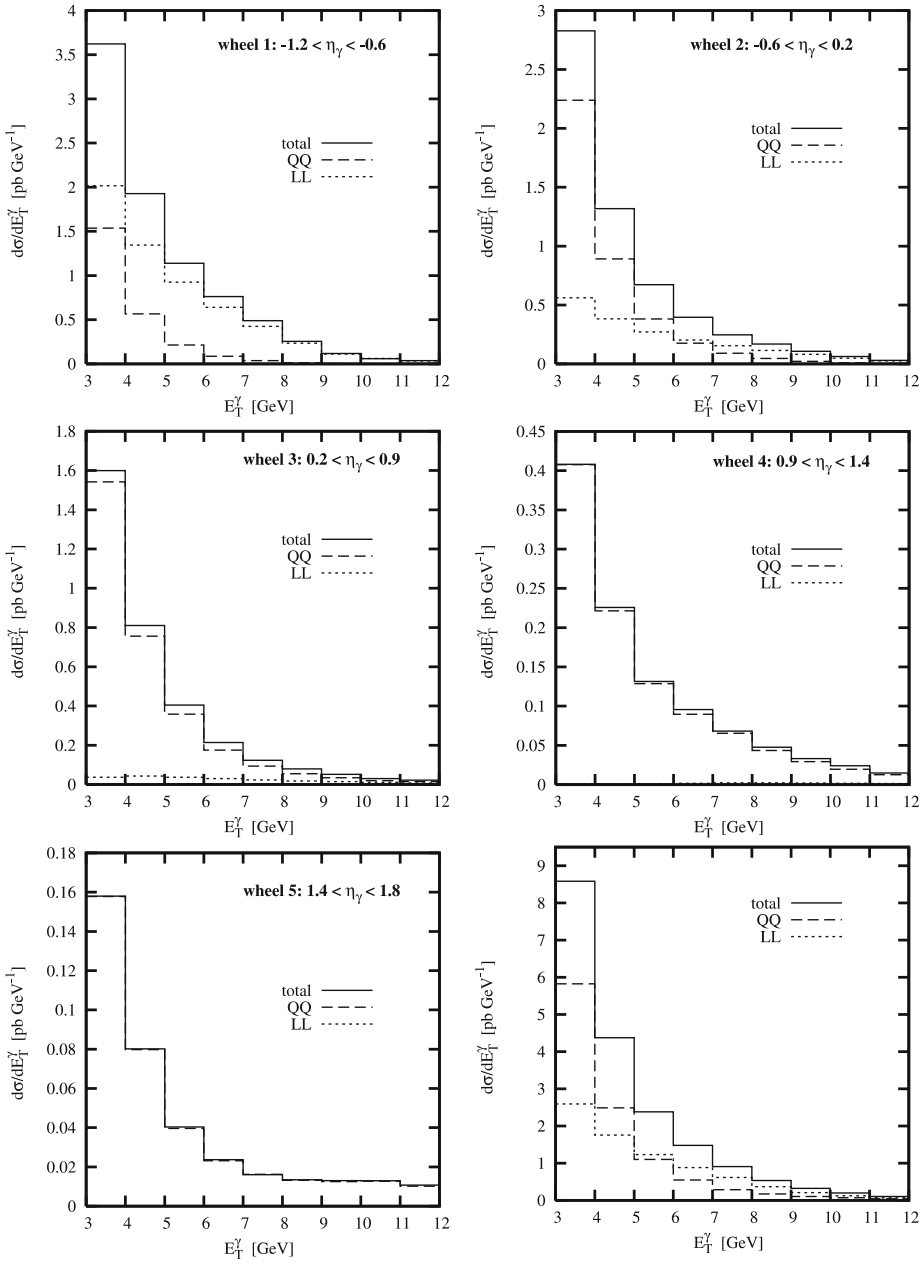

Fig. 7. Transverse energy distributions of isolated photons in $\gamma + (0+1)$-jet events, in different bins in η_γ. The *last plot* shows the sum over all bins. Isolated photons are defined here using the hadronic k_T-algorithm ($R = 1$), requiring $z > 0.9$. LL and QQ subprocess contributions are indicated as *dashed* and *dotted lines*

algorithm is the sum of the $\gamma + (0+1)$-jet and $\gamma + (1+1)$-jet cross sections. The inclusive isolated γ cross section and its decomposition into $\gamma + (0+1)$-jet and $\gamma + (1+1)$-jet final states is shown in Fig. 8. For the integrated cross sections, we obtain 19.1 pb for $\gamma + (0+1)$-jet, 27.6 pb for $\gamma + (1+1)$-jet and thus 46.7 pb for the inclusive cross section. This cross section is thus considerably larger than the inclusive isolated γ cross section obtained with the exclusive HERA-frame k_T-algorithm. As already discussed in Sect. 2.3, the latter algorithm is more likely to cluster photon and quark together into a single jet. Consequently, many final state configurations that were identified as photon jets with $z = 1$ by the hadronic k_T-algorithm yield photon jets with $z < 1$ with the exclusive HERA-frame k_T-algorithm. If these photon jets have $z < 0.9$, they do no longer contribute to the isolated photon cross section.

We observe that the $\gamma + (1+1)$-jet distributions fall less steeply than the $\gamma + (0+1)$-jet distributions, both in rapidity and in transverse energy. This feature can be understood from the fact that at large forward rapidity or at large transverse energy, it is kinematically preferred that the transverse energy of the photon is balanced by both the electron and the hard jet. Also, the $\gamma + (1+1)$-jet cross section exceeds the $\gamma + (0+1)$-jet everywhere in phase space. This might appear counter-intuitive at first sight, but may be understood from the fact that both cross sections start at the same order in perturbation theory, namely $\mathcal{O}(\alpha^3)$. The admixture of $\gamma + (0+1)$-jet and $\gamma + (1+1)$-jet events in the inclusive sample is highly dependent on the cuts applied to the quark jet, especially on its transverse energy cut, which is chosen here to be even lower than the cut on the transverse energy of the photon.

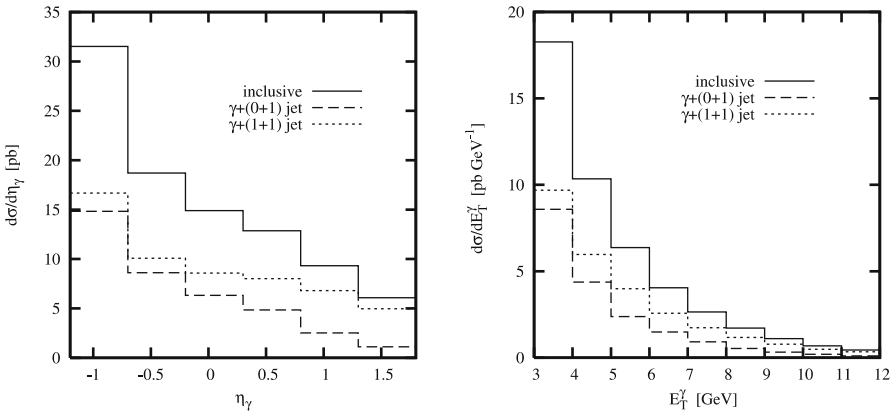

Fig. 8. Comparison of isolated $\gamma+(0+1)$-jet, $\gamma+(1+1)$-jet and inclusive isolated γ cross sections using the hadronic k_{T}-algorithm ($R=1$), requiring $z>0.9$

As a final point, we note that the measurement of the ZEUS Collaboration [21], based on a cone-based photon isolation, yielded an inclusive isolated photon production cross section considerably larger than the $\gamma+(1+1)$-jet cross section. This behaviour is due to the more restrictive cuts on the hadronic jet applied by ZEUS to select $\gamma+(1+1)$-jet final states. Both ZEUS measurements are in good agreement with the theoretical approach advocated here: we compared the inclusive isolated photon cross section with the ZEUS measurement in [21], and ZEUS compared [14] their measurement of the $\gamma+(1+1)$-jet cross section to an earlier NLO calculation [22], based on the same approach which we used here at leading order.

5 Conclusions and outlook

In this paper, we studied the production of final state photons in deep inelastic scattering at leading order in perturbation theory, $\mathcal{O}(\alpha^3)$. Already at this leading order, the corresponding parton-level cross section contains a collinear quark–photon divergence, which is absorbed into the quark-to-photon fragmentation function. Our calculation of final state photon production contains therefore both contributions from hard parton-level photon radiation and from photon fragmentation.

Besides a perturbatively generated component, the quark-to-photon fragmentation function contains a genuinely non-perturbative component, which forms the boundary condition to its perturbative evolution equation. Experimental measurements of this photon fragmentation function were made up to now only in electron–positron annihilation at LEP [3, 8].

In the democratic clustering procedure [7] for photon cross sections, the photon candidate is clustered by the jet algorithm like any hadron in the event. As a result, one of the final state jets contains a highly energetic photon, and is called photon jet, abbreviated by γ. Using this procedure, we studied the $\gamma+(0+1)$-jet production cross section in deep inelastic scattering at HERA, and demonstrated that the energy distribution of photons inside the photon jet in these events is highly sensitive on the quark-to-photon fragmentation function, and can be used to discriminate different available parametrisations of it. We could show that such a measurement is best carried out using a particular variant of the k_{T}-algorithm, which enhances the importance of fragmentation contributions relative to the hard radiation.

Isolated photons are usually defined at high energy experiments by allowing them to be accompanied by some amount of hadronic energy, since a perfectly isolated photon is not infrared safe in perturbation theory. The democratic clustering procedure allows for a natural definition of isolated photons by identifying the photon jet as isolated photon if the fraction of its energy carried by the photon candidate exceeds some value defined by the experimental environment. At HERA, photons are called isolated if they carry more than 90% of the transverse energy of the photon jet.

Using this definition, we studied isolated photon cross sections for $\gamma+(0+1)$-jet, $\gamma+(1+1)$-jet and inclusive γ final states for different jet algorithms. We found that particular features of the parton-level processes and of the jet algorithm can be related to aspects of the rapidity and transverse energy distributions of the photons.

As in our previous study of isolated inclusive photon production in deep inelastic scattering [21], based on a cone-based isolated criterion used in the corresponding experimental measurement [14], we found that photon radiation off the lepton and off the quark are of comparable importance, although either of them dominates in a different region in photon rapidity. This has important implications for the use of inclusive photon cross sections to measure the photon distribution in the proton [17, 19], as needed for electroweak corrections to hadron collider observables [18]. In particular, it invalidates the assumption [19] that the bulk of the isolated inclusive photon cross section in DIS arises only from photon radiation off the lepton, as already pointed out in [20, 21]. If possible at all, an extraction of the photon distribution in the proton would have to be restricted to kinematical regions where radiation off the lepton is indeed dominant.

NLO corrections, $\mathcal{O}(\alpha^3\alpha_{\mathrm{s}})$, are known to the $\gamma+(1+1)$-jet cross section in deep inelastic scattering [22] for some time already; this calculation was found to be in good agreement with experimental data recently [14]. The derivation of NLO corrections to the $\gamma+(0+1)$-jet cross section and the inclusive photon cross section in deep in-

elastic scattering is however considerably more involved. Owing to the appearance of the collinear quark–photon singularity in these observables already at leading order, an NLO calculation will encounter double unresolved partonic configurations, which are otherwise expected only at NNLO. In this sense, such a calculation would have similar features as the calculation of the NLO corrections to the $\gamma + 1$-jet rate at LEP [9], where first developments towards double unresolved real radiation were made.

Acknowledgements. We would like to thank Katharina Müller, Carsten Schmitz, Ulrich Straumann and David Saxon for many useful and clarifying discussions. This work was supported by the Swiss National Science Foundation (SNF) under contract PMPD2-106101.

References

1. K. Koller, T.F. Walsh, P.M. Zerwas, Z. Phys. C **2**, 197 (1979)
2. G. Altarelli, G. Parisi, Nucl. Phys. B **126**, 298 (1977)
3. OPAL Collaboration, K. Ackerstaff et al., Eur. Phys. J. C **2**, 39 (1998) [hep-ex/9708020]
4. D.W. Duke, J.F. Owens, Phys. Rev. D **26**, 1600 (1982)
5. M. Glück, E. Reya, A. Vogt, Phys. Rev. D **48**, 116 (1993); Erratum-ibid. D **51**, 1427 (1995)
6. L. Bourhis, M. Fontannaz, J.P. Guillet, Eur. Phys. J. C **2**, 529 (1998) [hep-ph/9704447]
7. E.W.N. Glover, A.G. Morgan, Z. Phys. C **62**, 311 (1994)
8. ALEPH Collaboration, D. Buskulic et al., Z. Phys. C **69**, 365 (1996)
9. A. Gehrmann-De Ridder, E.W.N. Glover, Nucl. Phys. B **517**, 269 (1998) [hep-ph/9707224]
10. A. Gehrmann-De Ridder, T. Gehrmann, E.W.N. Glover, Phys. Lett. B **414**, 354 (1997) [hep-ph/9705305]
11. A. Gehrmann-De Ridder, E.W.N. Glover, Eur. Phys. J. C **7**, 29 (1999) [hep-ph/9806316]
12. S. Frixione, Phys. Lett. B **429**, 369 (1998) [hep-ph/9801442]
13. J.E. Huth et al., Proceedings of Summer Study on High Energy Physics, Research Directions for the Decade, Snowmass, 1990; CDF Collaboration, F. Abe et al., Phys. Rev. D **45**, 1448 (1992); M. Seymour, Z. Phys. C **62**, 127 (1994)
14. ZEUS Collaboration, S. Chekanov et al., Phys. Lett. B **595**, 86 (2004) [hep-ex/0402019]
15. T. Sjöstrand, P. Edén, C. Friberg, L. Lönnblad, G. Miu, S. Mrenna, E. Norrbin, Comput. Phys. Commun. **135**, 238 (2001) [hep-ph/0010017]
16. G. Marchesini, B.R. Webber, G. Abbiendi, I.G. Knowles, M.H. Seymour, L. Stanco, Comput. Phys. Commun. **67**, 465 (1992)
17. M. Glück, C. Pisano, E. Reya, I. Schienbein, Eur. Phys. J. C **27**, 427 (2003) [hep-ph/0209335]; C. Pisano, doctoral thesis, Universität Dortmund (2005) [hep-ph/0512306]
18. H. Spiesberger, Phys. Rev. D **52**, 4936 (1995) [hep-ph/9412286]; M. Roth, S. Weinzierl, Phys. Lett. B **590**, 190 (2004) [hep-ph/0403200]
19. A.D. Martin, R.G. Roberts, W.J. Stirling, R.S. Thorne, Eur. Phys. J. C **39**, 155 (2005) [hep-ph/0411040]
20. D.H. Saxon, Proceedings of Ringberg Workshop New Trends in HERA Physics 2005, G. Grindhammer, B. Kniehl, G. Kramer and W. Ochs, World Scientific (Singapore, 2006), p. 177 [hep-ex/0601013]
21. A. Gehrmann-De Ridder, T. Gehrmann, E. Poulsen, Phys. Rev. Lett. **96**, 132 002 (2006) [hep-ph/0601073]
22. A. Gehrmann-De Ridder, G. Kramer, H. Spiesberger, Phys. Lett. B **459**, 271 (1999) [hep-ph/9903377]; Nucl. Phys. B **578**, 326 (2000) [hep-ph/0003082]
23. L.E. Gordon, W. Vogelsang, Phys. Rev. D **52**, 58 (1995); M. Krawczyk, A. Zembrzuski, Phys. Rev. D **64**, 114 017 (2001) [hep-ph/0105166]; M. Fontannaz, J.P. Guillet, G. Heinrich, Eur. Phys. J. C **21**, 303 (2001) [hep-ph/0105121]; Eur. Phys. J. C **26**, 209 (2002) [hep-ph/0206202]
24. ZEUS Collaboration, J. Breitweg et al., Phys. Lett. B **472**, 175 (2000) [hep-ex/9910045]; H1 Collaboration, A. Aktas et al., Eur. Phys. J. C **38**, 437 (2005) [hep-ex/0407018]
25. D.Y. Bardin, C. Burdik, P.C. Khristova, T. Riemann, Z. Phys. C **42**, 679 (1989)
26. W.T. Giele, E.W.N. Glover, Phys. Rev. D **46**, 1980 (1992)
27. B. Badelek, J. Kwieciński, Phys. Lett. B **295**, 263 (1992); Rev. Mod. Phys. **68**, 445 (1996) [hep-ph/9408318]
28. U. Baur, J.A.M. Vermaseren, D. Zeppenfeld, Nucl. Phys. B **375**, 3 (1992)
29. European Muon Collaboration, J.J. Aubert et al., Phys. Lett. B **218**, 248 (1989)
30. G. Curci, W. Furmanski, R. Petronzio, Nucl. Phys. B **175**, 27 (1980); W. Furmanski, R. Petronzio, Phys. Lett. B **97**, 437 (1980), Z. Phys. C **11**, 293 (1982)
31. A. Gehrmann-De Ridder, G. Kramer, H. Spiesberger, Eur. Phys. J. C **11**, 137 (1999) [hep-ph/9907511]
32. J. Pumplin, D.R. Stump, J. Huston, H.L. Lai, P. Nadolsky, W.K. Tung, JHEP **0207**, 012 (2002) [hep-ph/0201195]
33. C. Schmitz, private communication
34. H1 Collaboration, C. Adloff et al., Eur. Phys. J. C **19**, 289 (2001) [hep-ex/0010054]
35. H1 Collaboration, C. Adloff et al., Eur. Phys. J. C **19**, 429 (2001) [hep-ex/0010016]
36. S.D. Ellis, D.E. Soper, Phys. Rev. D **48**, 3160 (1993) [hep-ph/9305266]
37. S. Catani, Y.L. Dokshitzer, M. Olsson, G. Turnock, B.R. Webber, Phys. Lett. B **269**, 432 (1991)
38. S. Catani, Y.L. Dokshitzer, B.R. Webber, Phys. Lett. B **285**, 291 (1992)
39. S. Catani, M. Fontannaz, J.P. Guillet, E. Pilon, JHEP **0205**, 028 (2002) [hep-ph/0204023]
40. T. Binoth, J.P. Guillet, E. Pilon, M. Werlen, Phys. Rev. D **63**, 114 016 (2001) [hep-ph/0012191]